ELSEVIER

Polymer 41 (2000) 8801–8812

polymer

www.elsevier.nl/locate/polymer

# A study of the morphologies and growth kinetics of three monodisperse *n*-alkanes: $C_{122}H_{246}$, $C_{162}H_{326}$ and $C_{246}H_{494}$

I.L. Hosier, D.C. Bassett*

*Department of Physics, J. J. Thomson Physical Laboratory, University of Reading, Whiteknights, P.O. Box 220, Reading RG6 6AF, UK*

Received 12 October 1999; received in revised form 28 December 1999; accepted 29 December 1999

**Abstract**

An optical and electron microscopic study has been made of three monodisperse *n*-alkanes crystallising as extended-chain lamellae. All showed similar morphologies at the same supercooling and the same progressive changes of texture with crystallization temperature. This is, with increasing supercooling, from a morphology composed essentially of individual lamellae arranged in parallel stacks and radiating from common nuclei through coarse, somewhat branched microstructures whose parallel stacks diverge, to finer, more-branched pseudo-spherulitic textures. Quenched, once-folded, $C_{246}$ shows a random spherulitic texture with a dominant/subsidiary microstructure as for polymeric systems. The kinetics of extended-chain growth increase linearly with supercooling, as predicted by Hoffman, except for a local dip at the onset of lamellar branching. This new phenomenon occurs within one quantized state of lamellar thickness in contrast to 'self-poisoning' when once-folded forms give way to extended-chain crystallization. When dominant lamellae are no longer parallel but diverge, their mutual splaying angles increase with supercooling for all the three *n*-alkanes studied. The values are less, for the same supercooling, for the longer homologues with their thicker lamellae. This behaviour is as expected of transient ciliation due to the excess of molecular length over that of the secondary nucleus and thereby reinforces previous evidence demonstrating the responsibility of ciliation for spherulitic development in polymers. 

*Keywords*: Monodisperse *n*-alkanes; Extended-chain crystallization kinetics; Ciliation

## 1. Introduction

Characteristically polymeric properties derive ultimately from the length of their constituent molecules so that it is logical to base an understanding of their structure–property relationships on knowledge of how molecular length affects properties starting with oligomeric materials, i.e. the *n*-alkanes for polyethylene. It was Andrew Keller's opinion [1] that the study of *n*-alkanes 'should enable us to put many aspects (of polymeric organization) which previously could only be approached speculatively on a firmer ground'. To this end he investigated a number of these paraffins soon after the discovery of polymer single crystals, notably hexatriacontane, $C_{36}H_{74}$ [2,3], finding helpful analogies of non-planar habits [4] between them and linear polyethylene. More recently, he was instrumental in bringing about the synthesis of monodisperse long *n*-alkanes by Whiting and colleagues [5,6] in which no homologues are detectable.

Our particular interest in these special materials relates to the possibility of using them to test previous predictions of the cause of spherulitic growth, the characteristic way in which synthetic polymers crystallize from the melt, which imply that this, too, is a consequence of molecular length.

The first systematic electron microscope studies of the internal lamellar morphology of melt-crystallized polymers showed that spherulites were constructed on a framework of individual dominant lamellae, which tended to diverge at near-constant angle. It was, accordingly, proposed [7–9] that the origin of lamellar divergence is a mesoscopic short-range repulsive force operative in the region of a branch point. This follows from the linear traces of the lamellae. Because such flexible objects can be made to bend through a right angle in particular circumstances [10] the linearity demonstrates that they did not grow under stress and that the mutual divergence takes place close to the branch point. As the distances involved do not exceed the molecular length, it was proposed [7–9] that the short-range force is due to pressure of the dynamic molecular cilia during growth.

This is envisaged in the following way. Until a molecule is able to add completely to a layer, substantial portions will lie outside and adjacent to the fold surfaces. There they will

* Corresponding author. Tel.: +44-118-931-8540; fax: +44-118-975-0203.

*E-mail address:* d.c.bassett@reading.ac.uk (D.C. Bassett).

0032-3861/00/$ - see front matter 
PII: S0032-3861(00)00223-8

be unable to diffuse away but will occupy space and exert a repulsive pressure, with a weak rubbery modulus, on any competitor for that space. This will be pertinent especially at the start of a new layer when molecules adding to its side surfaces will tend to be in the way of the emerging lamella that will, in effect, repel itself from the mother layer. Adjacent lamellae will, therefore, tend to be forced apart during growth and, given a distribution of branch points in space, iteration will produce the spherical envelope around equivalent radial units of a mature spherulite. Work on the *n*-alkanes has, as described below, emphasized how close to the branch point these influences are at work.

The existence of a mesoscopic short-range force for polymeric growth is demonstrated unambiguously from the geometry of spiral terraces in multilayer crystals within a quenched matrix [11]. Adjacent layers that have developed around the (etched-out) giant screw dislocation are not in contact showing that divergence is not a nucleation phenomenon but a distortion of lamellae away from adjacency and crystallographic continuity in the third dimension.

The monodisperse *n*-alkanes presented the first opportunity for a critical test of the proposed role of ciliation. Earlier X-ray studies [12] had shown that these systems tended to crystallize with the methyl end groups confined to the basal surfaces resulting in quantized thicknesses of the extended-chain length (in projection) or an integral submultiple thereof. In practice, there are departures from strict quantization, as would be expected for the small contribution surface packing makes to the total free energy of the system but the concept, nevertheless, offers a convenient classification of the crystallized systems.

For melt growth of alkanes with $> \sim 200$ C atoms, the kinetics pass through a minimum with increasing supercooling; above this temperature the extended form predominates, below it the once-folded [13,15]. To the approximation that molecular stems add as units to the crystal, one would expect no cilia—and hence no spherulites—for the extended form but spherulites should occur for the once-folded form because of the presence of (transient) cilia of half the molecular length. This simple prediction is borne out [14,15] for growth close to the kinetic minimum in $C_{294}H_{590}$.

The corresponding microstructure changes from diverging dominant lamellae and later-forming subsidiaries, as in polymer spherulites, to extensive parallel arrays of extended-chain lamellae [15,16]. The change in morphology not only confirms the essential role of ciliation but also demonstrates that, to operate for alkanes, the range of the associated force must be much less than could be inferred for polymers. For cilia no more than several nm long, the implication is that splaying is effected very close to the branch point, so close that molecules partly attached to the nearby lateral growth surfaces would provide effective repulsion from the neighbouring basal surfaces.

The simple correlation between the occurrence of spherulites with characteristic microstructure and chain-folding and its absence for extended-chain growth only holds to the approximation that molecules add to the crystal as integral stems. Our preliminary studies of *n*-alkanes beginning with $C_{98}H_{196}$, which only crystallize in extended-chain form, show that it begins to fail progressively as crystallization temperature is lowered [16]. A kind of coarse spherulite ensues, without the equivalent radii of the classic spherulite, showing wide sectors of the same orientation but becoming finer at lower temperatures. Their dominant lamellae also diverge repetitively, especially near the origin, indicating that they, too, have been subject to a short-range repulsive force. However, they possess a substructure of parallel lamellae, appropriate to the optical coarseness, rather than the dominant/subsidiary construction typical of polymeric spherulites. The present work investigates this phenomenon further and shows that the detailed behaviour conforms to expectations based on the presence and responsibility of transient ciliation deriving from the excess of molecular length over that of the relevant nucleus. In addition, it confirms the reality of the previously noted [16] temporary dip in growth kinetics at the onset of branching, which otherwise are linear with supercooling as predicted [17].

## 2. Experimental

### 2.1. General handling precautions

Paraffins, by their very nature, require specialised handling procedures. Extreme care must be taken not to contaminate these very pure materials with any other organic substance (especially other polymers). Moreover, only small amounts of these monodisperse materials are available. Both these factors require a much higher level of care to avoid contamination than is normally necessary when dealing with conventional polyethylenes.

### 2.2. Thermal analysis

A Perkin–Elmer DSC-2C differential scanning calorimeter (DSC) was used to examine the crystallization and melting behaviour. Prior to use it was calibrated for both isothermal and scanning runs, using a four point calibration with a cubic extrapolation, against pure lead, tin, indium and stearic acid,. For each run, about 1–2 mg of the paraffin was placed into a fresh aluminium DSC pan. The samples were crystallized in the DSC after first holding the paraffin at its melting point for 1 min and then lowering the temperature, at 40 K $min^{-1}$, to that required for crystallization. Following crystallization, samples were quenched to room temperature. The corresponding melting endotherms were obtained at a heating rate of 20 K $min^{-1}$. To avoid any problems of degradation, each fresh sample of paraffin was used for a maximum of two crystallization–melting runs.

### 2.3. Optical microscopy and kinetics

Both kinetic measurements and optical micrographs were

Table 1
Key data for $C_{122}$ (all specimens were melted at 124°C prior to crystallization)

| Crystallization temperature (°C) | Growth rate ($\mu m\ s^{-1}$) | Crystallization time | Object diameter ($\mu m$) | Melting peak (°C) | Form |
|---|---|---|---|---|---|
| Quenched | | | 40–50 μm | 121.1 | ext. |
| 116.0 | 11.0 ± 0.4 | 4–6 s | 100 | 120.7 | ext. |
| 116.5 | 10.7 ± 0.3 | 6–8 s | 100–120 | | ext. |
| 117 | 10.6 ± 0.3 | 8–10 s | 130–140 | 120.9 | ext. |
| 117.5 | 9.3 ± 0.2 | 10–12 s | 140–150 | | ext. |
| 118 | 7.3 ± 0.3 | 15–18 s | 160–180 | 120.9 | ext. |
| 118.5 | 5.3 ± 0.2 | 20–22 s | 180–220 | | ext. |
| 119.0 | 4.0 ± 0.3 | 40–55 s | 270–310 | 120.8 | ext. |
| 119.2 | 3.0 ± 0.1 | 2–5 min | 600–800 | | ext. |
| 119.4 | 1.6 ± 0.02 | 6–10 min | 1–2 mm | 120.6 | ext. |

obtained from the same specimens viewed on a Mettler FP80 hot-stage. Some 5 mg of paraffin was placed between clean microscope slide and cover-slip and the whole inserted into the stage under a nitrogen atmosphere. The material was melted for 1 min and then cooled to the crystallization temperature at 40 K $min^{-1}$ (to parallel the DSC procedure). At the end of the crystallization time the slide was effectively quenched by being placed on a cold surface.

In situ imaging of growing crystals was accomplished by mounting the FP80 hot-stage between crossed polars on a Zeiss universal microscope and using a small CCD camera for video recording as crystal growth proceeded. Kinetic data were obtained directly from the recorded data by marking the positions of the tips of individual crystals as a function of time, and taking the gradient of the fitted curve. In all the paraffins mentioned here, growth rates were linear with time until impingement, consequently only the average growth rate data is shown. The growth rate data can also be used to calculate the crystallization time, provided the final lamellar dimensions are known; in all cases these calculated values corresponded with the crystallization times recorded from the DSC. The kinetic data points were each an average of around 20 different crystals in at least two independent areas of each specimen at any one temperature.

Optical micrographs were taken on a Zeiss GFL transmission microscope, between crossed polars, immediately after full crystallization; magnifications were calibrated against a standard graticule.

### 2.4. Transmission electron microscopy (TEM)

To avoid beam damage, carbon replicas of permanganically-etched surfaces were examined instead of the actual samples directly. The best procedure to prepare these replicas for materials of very limited availability was to crystallize the paraffin within a 5 mm diameter gold TEM grid (200 mesh) and then take a direct replica. About 2 mg of the paraffin was placed on the TEM grid itself sitting on a microscope slide and pre-melted on a Kofler hot-bench to remove included air. A pre-warmed cover-slip was then placed on top and the entire assembly placed inside a Mettler FP80 hot-stage for crystallization, as detailed above. After quenching, the cover-slip was gently prised off leaving the grid and paraffin adhering to the microscope slide. The combination was etched for 5 min in a pool of etchant (1% $KMnO_4$ in a 10:4:1 mixture of sulphuric acid, phosphoric acid and water, respectively), which was replaced halfway through. Etching was quenched using a 1:4 mixture of hydrogen peroxide in a 2:7 mixture of sulphuric acid in water, which had been pre-cooled over dry ice for at least 10 min beforehand. Subsequently the quenched etchant was removed by gently running methanol over the grid after which the etched grid was gently lifted from the slide and allowed to dry.

To prepare replicas, tungsten/tantalum metal was evaporated at a nominal angle of 35° to the horizontal, followed by vertical carbon coating, directly on the etched grids. The paraffin was removed from the replica by refluxing in boiling xylene leaving the grids ready for TEM examination.

### 2.5. X-ray procedure

Small-angle X-ray scattering, SAXS, was used to measure the average crystal thickness and so confirm whether the alkane molecules were extended or folded within the crystalline lamellae. The single diffraction ring generally obtained was consistent with molecules being inclined at $\sim 35°$ to lamellar normals.

### 2.6. Splaying-angle measurements

The splaying-angle between two adjacent planar dominant lamellae is that by which either needs to be rotated, about their common axis (line of intersection), to bring their planes into coincidence. Measurement of this quantity is complicated by the range of different lamellar orientations generally present on a single micrograph. These problems can be reduced by identifying lamellae in edge-on orientation to the print, checking this assignment by rotation about the projected length if necessary, then measuring a large number of such angles across the sample. This does not remove necessarily any systematic errors due to the common axis being non-normal to the page, but with careful selection the mean should be little biased. In the

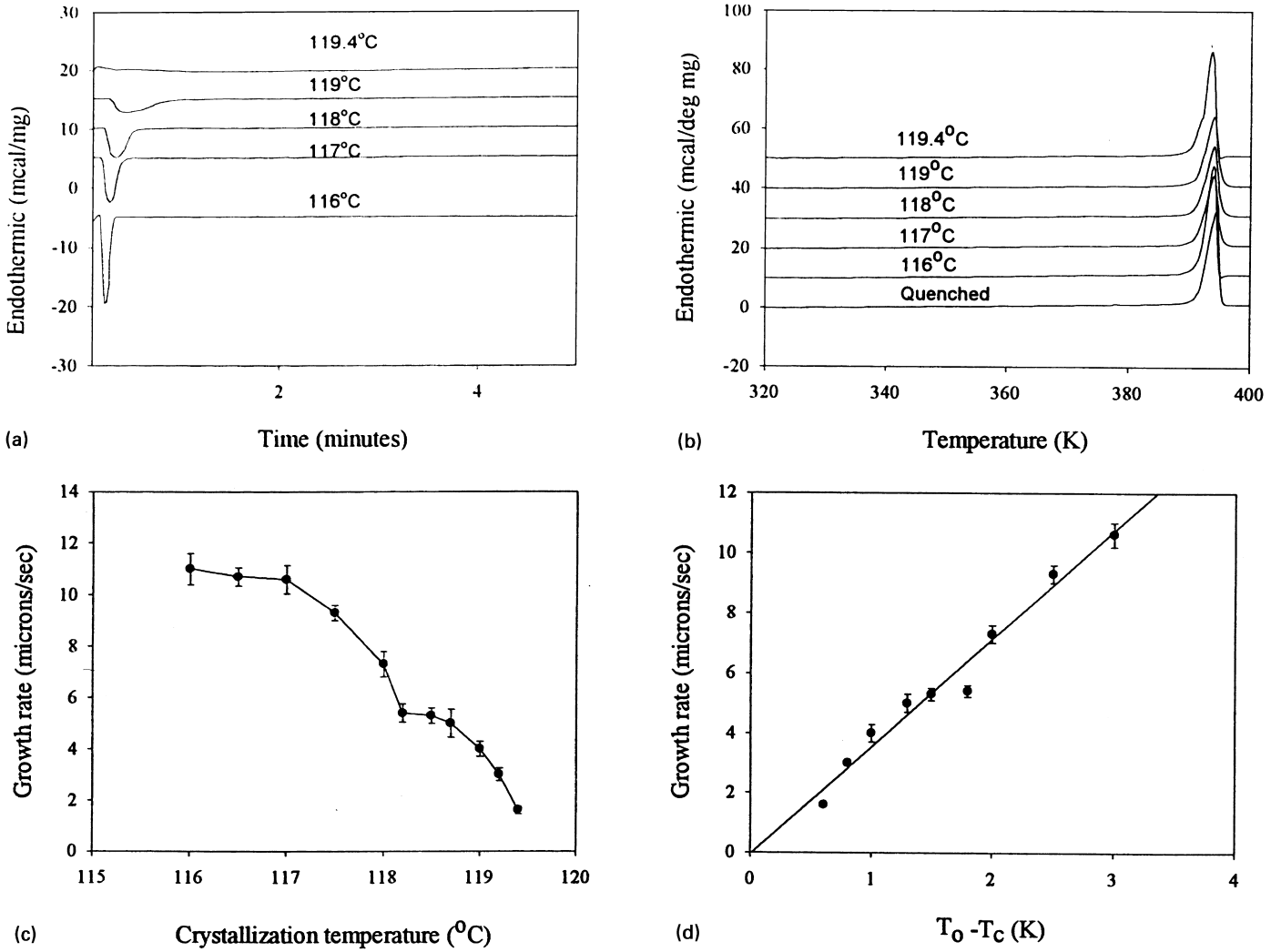


Fig. 1. Crystallization behaviour of $C_{122}$: (a) crystallization exotherms; (b) melting endotherms; (c) growth rate plotted as a function of crystallization temperature; and (d) growth rate plotted as a function of supercooling.

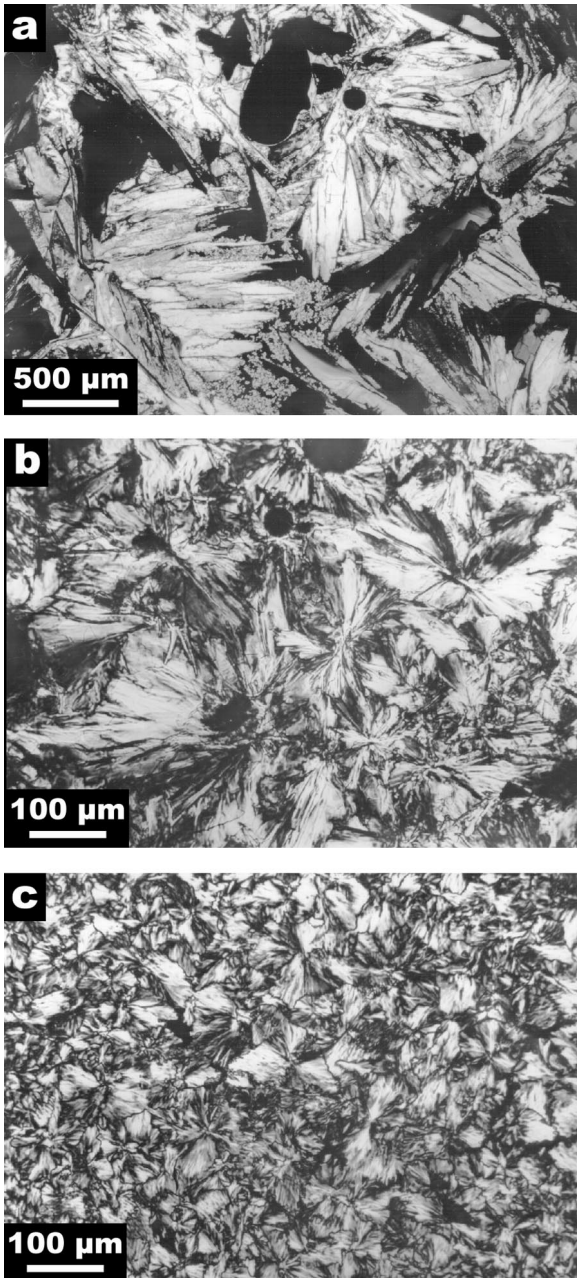


Fig. 2. Optical micrographs of $C_{122}$: (a) structure based on parallel groups of lamellae after crystallizing at 119.2°C; (b) disordered texture after crystallizing at 119°C; and (c) pseudo-spherulitic texture after quenching.

comparative data included here about 20 angles were measured for each sample allowing an average to be calculated together with a standard deviation.

## 3. Results

### 3.1. $C_{122}H_{246}$ n-alkane

A full set of numerical data for this material is listed in Table 1.

#### 3.1.1. DSC and crystallization behaviour

The crystallization exotherms are shown in Fig. 1a, vertically displaced for clarity. At lower temperatures the time for total crystallization increases with temperature from ~5 s at 116°C to ~15–20 s at 118°C. At 116°C there is an appreciable negative transient recorded by the DSC during the cooling process, even after baseline correction, which suggests that a proportion of the material is crystallizing non-isothermally. At higher temperatures the crystallization time becomes progressively longer, being almost 10 min at the highest temperature of 119.4°C.

The corresponding melting endotherms are shown in Fig. 1b. All the melting temperatures correspond to one another within the experimental uncertainty (±0.3 K). They are close to the accepted value of 121.5°C calculated from Broadhurst's data [18]. The melting points do not change systematically with crystallization temperature. A small low-temperature shoulder is present for crystallization at the highest temperature. It is possible that this is due to a small proportion of more highly sheared lamellae in line with Keller's early observations [3]. He found that, close to the melting point, ridges appeared on the basal surfaces of crystals of short *n*-alkanes, such as $C_{36}H_{74}$, within which the chain inclination to the lamellar normal had increased. Such states of higher shear would melt at lower temperatures because of their increased specific surface area and reduced lamellar thickness.

#### 3.1.2. Kinetic measurements

Fig. 1c shows the growth rates in $\mu m\ s^{-1}$ plotted against the crystallization temperature; the width of the calculated standard error on each point indicates the typical uncertainty associated with each measurement. There is a local minimum of crystallization rate at 118°C associated with morphological consequences as discussed later.

Otherwise, a straight line can be fitted through all but two of the experimental points, in support of Hoffman's theory [17]. As the specific prediction is that growth rate increases linearly with supercooling, Fig. 1d is a plot of the experimental data in this form. A straight line with gradient 3.65 $\mu m\ s^{-1}\ K^{-1}$ fits all the data points to within one standard deviation except for the two for the lowest temperatures (omitted) for which non-isothermal growth is believed to be the cause; the sample tends to crystallize mainly during the cooling process. This behaviour sets a lower limit on the accessible temperature range at which any paraffin can be crystallized in a true isothermal regime. For $C_{122}$ in our experiments, this range is 117–119.4°C and is determined by the thermal mass of the hot-stage and maximum cooling rate. The maximum growth rate recorded for this paraffin is $11.0 \pm 0.4\ \mu m\ s^{-1}$, while the supercooling required to initiate growth is ~2 K; in this the growth rate and DSC data were entirely consistent.

#### 3.1.3. SAXS

The SAXS data confirm that this paraffin crystallizes in

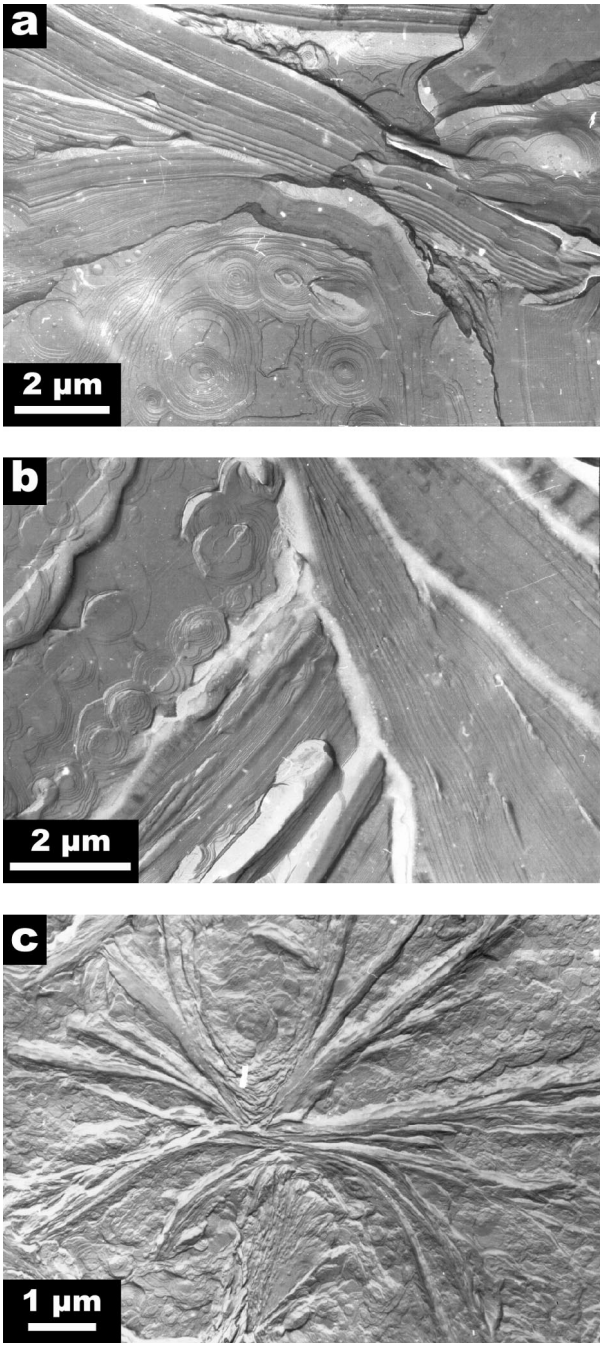


Fig. 3. TEM images of $C_{122}$: (a) morphology produced by crystallizing at 119.2°C; (b) microstructure mainly composed of lamellar bundles produced by crystallizing at 118°C; and (c) example of divergent object produced by quenching.

the extended-chain conformation with a crystal thickness of 13.0 ± 0.5 nm and a chain tilt of 33 ± 2°.

*3.1.4. Morphology*

The sequence of photomicrographs in Fig. 2 shows the progression from a multiply-nucleated single crystal type of morphology at low supercoolings to an increasingly spherulitic texture at lower crystallization temperatures. The former, (Fig. 2a), have the characteristic and familiar shape—elliptic (in the botanical sense) with acuminate tips—reported in the earlier studies [15,16]. This gives way, at the local minimum in growth rate mentioned above, to a branching texture in which dominant lamellae splay apart, increasingly so at still lower temperatures until, after quenching (Fig. 2c), a type of spherulitic texture ensues. This radiates from the central nuclei but lacks the equivalent radii of the classic spherulites; instead of the 'Maltese cross' pattern with well-defined azimuthally alternating four bright and four dark regions, one finds rather ill defined quadrants with many crystals appearing to radiate outwards parallel to one another. Intermediate textures, e.g. after crystallizing at 119°C (Fig. 2b), contain larger objects with wide sectors of parallel crystals often lacking spherical symmetry.

Corresponding TEM images are in Fig. 3 with Fig. 3c showing features in a quenched specimen. The lamellae initially diverge at relatively large angles (~16°) and are then planar. At higher crystallization temperatures, groups of parallel or near parallel lamellae are present throughout the sample (Fig. 3b, 118°C), both in edge-on and flat-on profiles. When crystallized at 119.2°C (Fig. 3a) the entire sample is composed of such organized parallel arrays of crystals, which now show smaller divergence angles (~10°), with many crystals not diverging at all.

*3.2. $C_{162}H_{326}$ n-alkane*

A full set of numerical data for this material is listed in Table 2.

*3.2.1. DSC and crystallization behaviour*

The crystallization exotherms shown as Fig. 4a reveal similar behaviour to $C_{122}$. Crystallization times, measured by DSC, range from a few seconds at 121°C (near quenching) to 10 min at 124°C; non-isothermal crystallization begins to occur at 120°C. All samples melt at 126.5 ± 0.3°C. A small low-temperature shoulder is present on the main peak for crystallization at 124°C, akin to that observed in $C_{122}$.

*3.2.2. Kinetic data*

The data in the graph of Fig. 4c can be fitted by a single straight line through all but one of the points; for this, at 120°C, much of the crystallization occurs during cooling. There is also a local minimum at around 123°C. However, compared to $C_{122}$ the maximum growth rate is reduced to around 6–7 $\mu m\, s^{-1}$; a reduction is to be expected for a longer paraffin. Despite these subtle differences, the overall growth and crystallization behaviour is qualitatively similar to that of $C_{122}$.

*3.2.3. SAXS*

X-ray data show that for all the crystallization temperatures considered here, $C_{162}$ is in the extended form with a

Table 2
Key data for $C_{162}$ (this paraffin was melted at 129°C)

| Crystallization temperature (°C) | Growth rate ($\mu m\ s^{-1}$) | Crystallization time | Object diameter ($\mu m$) | Melting peak (°C) | Form |
|---|---|---|---|---|---|
| Quenched | | | 20–40 | 126.7 | ext. |
| 120 | 5.5 ± 0.1 | 5–8 s | 40–50 | 126.3 | ext. |
| 121 | 5.6 ± 0.2 | 8–12 s | 60–70 | 126.3 | ext. |
| 122 | 4.5 ± 0.1 | 20–25 s | 80–110 | 126.5 | ext. |
| 123 | 2.3 ± 0.1 | 35–45 s | 150–200 | 126.7 | ext. |
| 123.5 | 1.76 ± 0.05 | 1–2 min | 300–400 | 126.6 | ext. |
| 124 | 0.83 ± 0.03 | 7–10 min | 500–700 | 126.8 | ext. |

crystal thickness of 16.7 ± 0.7 nm with a chain tilt of 34 ± 2°.

*3.2.4. Morphology*

Photomicrographs of this paraffin crystallized at various temperatures are presented in Fig. 5. A higher nucleation density has given this paraffin a finer texture than the previous one but the same sequence of habits recurs. Single crystals grow at 124°C (Fig. 5a), giving way to a coarse, branched morphology at 122°C (Fig. 5b) and spherulitic type objects (Fig. 5c) on quenching, very similar to those observed in $C_{122}$ after quenching. This general scheme of morphology is in line with that seen in the previous paraffin, including the onset of branching, at ~123°C, accompanying the local minimum in growth rates.

Lamellar detail is present in the TEM images of Fig. 6. In Fig. 6c, a characteristic object produced by quenching has a set of planar lamellae diverging from the origin at ~17° in places Lamellar divergence decreases with rising crystallization temperature; compare objects grown at 122°C (Fig. 6b) with those in Fig. 6a, which shows regions of crystal stacks diverging at low angles in a sample crystallized at 123°C.

*3.3. $C_{246}H_{494}$ n-alkane*

A full set of numerical data for this material is listed in Table 3.

*3.3.1. DSC and crystallization behaviour*

This alkane differs from its two predecessors in that it is the only one studied that is able to adopt both the extended and once-folded conformations. The latter has occurred only on quenching; isothermal growth gives the extended form (Fig. 7a). Isothermal crystallization can be maintained down to 123°C, giving a much wider range of possible crystallization temperatures than hitherto. Furthermore, the time scales for crystallization are much greater than before, being in excess of an hour for crystallization at the highest temperature, 128°C. Corresponding melting endotherms are shown in Fig. 7b. The lowest trace is to be interpreted as the melting of a crystal population composed of folded chains, which recrystallizes into the extended form during the scan in agreement with other work [19]. This explanation is confirmed by the facts that the total enthalpy of the polymer is contained in the second peak (at 131.5°C) where the extended form melts and that the once-folded melting and re-crystallization peak areas are identical. A small peak due to once-folded molecules in the higher temperature endotherms may well be a result of less stable crystallization, possibly caused by subsidiary material trapped between crystals in agreement with the earlier TEM studies [20].

*3.3.2. Kinetic data*

Growth rates calculated from direct observations of single crystals are shown in Fig. 7c. The overall shape of the graph is similar to those discussed previously, but with a growth rate reduced by as much as an order of magnitude. In this material the change in the growth behaviour at lower temperatures marks the onset of the once-folded form preparatory to the kinetic minimum at 122°C [13]; it is *not* the result of non-isothermal crystallization as previously described for the other paraffins. The local minimum associated with the onset of branching is apparent at 127°C.

*3.3.3. SAXS*

In confirmation of the DSC data, SAXS does confirm the existence of a once-folded state of this polymer after quenching with a crystal thickness of 14.7 ± 1.9 nm and an estimated chain tilt of 21 ± 3°. This figure is less than the ~35° expected and may be a consequence of the difficulty of taking the thickness of the fold region accurately into account. For all isothermal crystallization temperatures, the extended form predominates with crystal thickness of 26.7 ± 3.7 nm and a chain tilt of 32 ± 3°.

*3.3.4. Morphology*

The photomicrographs of Fig. 8 show, in Fig. 8a, a morphology composed of very coarse radiating groups for the highest crystallization temperature (128°C). Where crystals lie flat-on they can be seen to have the characteristic habit with curved prism faces. At intermediate crystallization temperatures (124°C, Fig. 8b), this gives way to broad parallel arrays of lamellae within a spherical envelope radiating from the single nucleation points. Fine spherulitic objects with well-defined Maltese crosses are formed on quenching (Fig. 8c). These are markedly different from

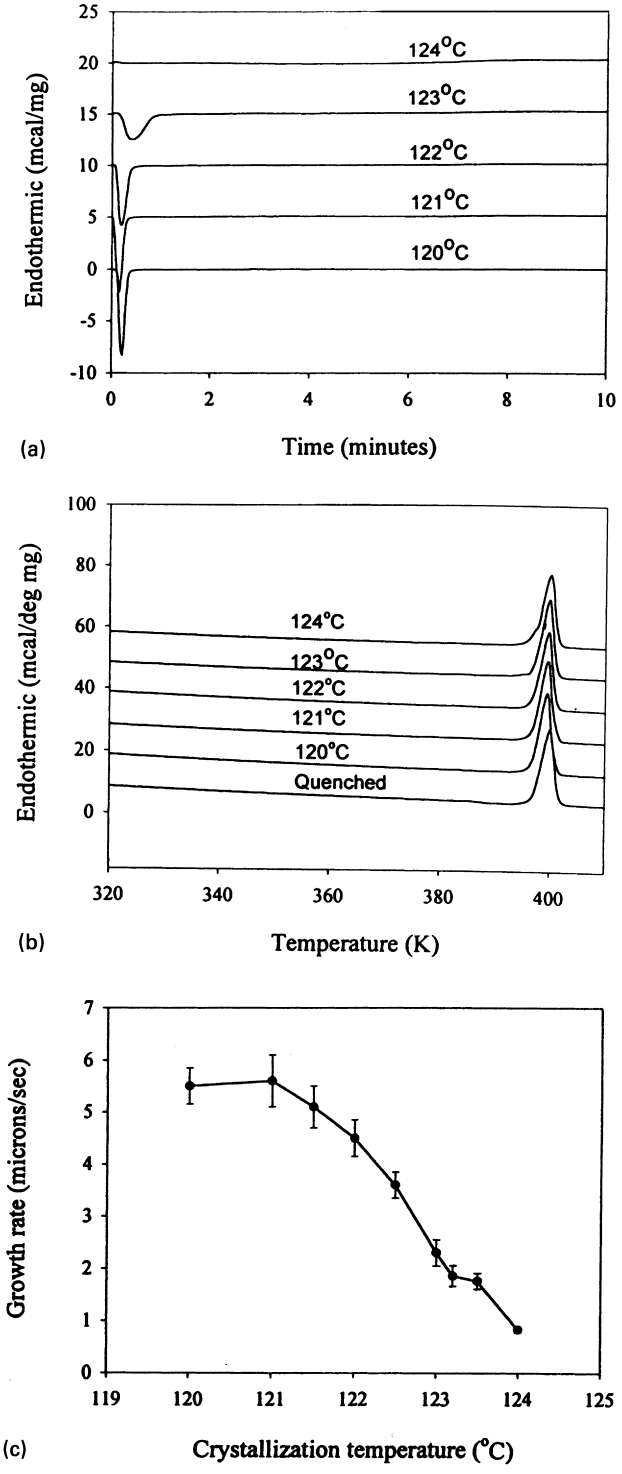


Fig. 4. Crystallization behaviour of $C_{162}$: (a) crystallization exotherms; (b) melting endotherms; and (c) growth rate plotted as a function of crystallization temperature.

the quenched forms of the other paraffins (compare Fig. 8c with Figs. 2c and 5c). Apart from the quenched form composed of folded chain crystals, the microstructure follows the general pattern behaviour encountered previously in the shorter homologues.

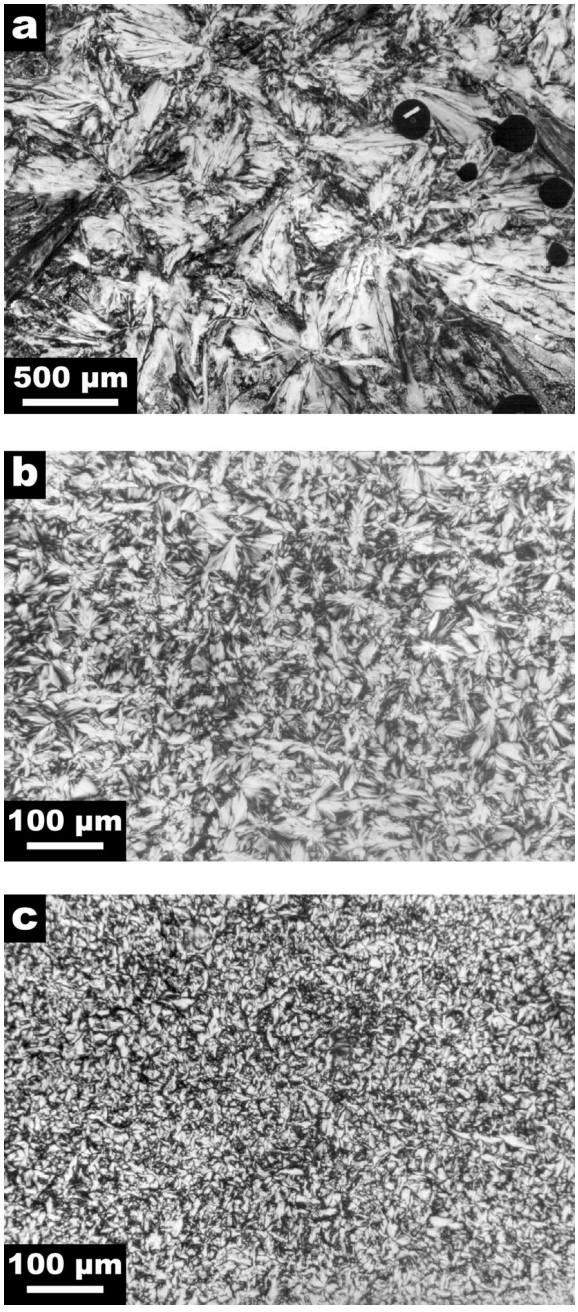


Fig. 5. Optical micrographs of $C_{162}$: (a) structure based on disordered groups of lamellae after crystallizing at 124°C; (b) intermediate texture after crystallizing at 122°C; and (c) pseudo-spherulitic texture after quenching.

The lamellar detail of Fig. 9 brings out the differences between the various morphologies. After crystallizing at 127°C, the morphology is the one of predominately parallel crystal stacks, (see Fig. 9a) with branching angles ~10°. By contrast, in the quenched specimen (Fig. 9c) the morphology is one of classical divergent sheaves. Unlike objects seen in the earlier paraffins, these show a degree of large angle (>20°) divergence even away from any obvious branch points (compare Figs. 3c and 6c) and resemble textures familiar in conventional polyethylene. At

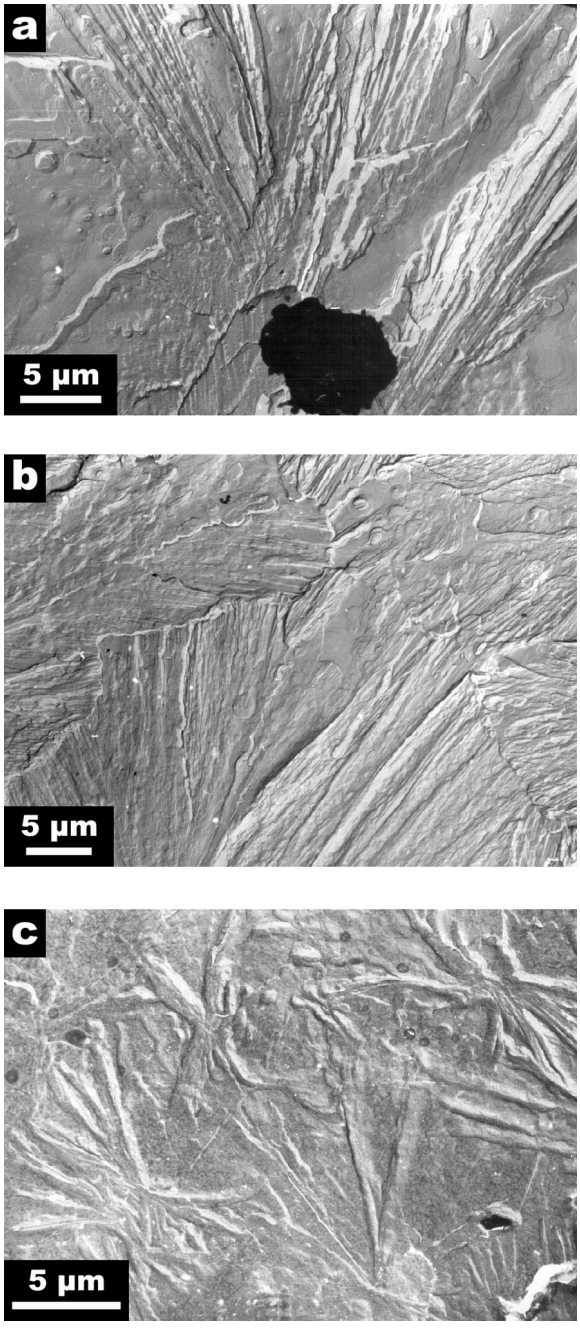


Fig. 6. TEM images of $C_{122}$: (a) morphology composed mainly of lamellar groups produced by crystallizing at 123°C; (b) detail of low angle divergent microstructure produced by crystallizing at 122°C; and (c) compact, divergent objects produced by quenching.

intermediate crystallization temperatures, morphologies built on lamellae diverging at low angle become more prevalent; compare the divergence angles in Fig. 9c with Fig. 9b.

## 4. Discussion

The results reported here not only support the existing theory but also reveal a new kinetic phenomenon as well as supporting the developing understanding of the causes of spherulitic growth in polymers. The first point is that the overall linear increase of growth rate with supercooling agrees with the prediction of Hoffman's theory [17]. Secondly, the kinetic dip, first seen for *n*-$C_{98}H_{196}$ [16], by recurring in three further systems as reported here, is undoubtedly real. It is a new phenomenon whose significance has still to be established.

Contrary to the earlier kinetic minima reported in several systems when extended-chain crystallization gives way to once-folded [13,21] that represents interference between two quantized states, we are now seeing a minimum within one quantized state. Its coincidence with the onset of branching, which will cause a proliferation of lamellae, suggests that the boundary conditions for some transport process are thereby changed significantly. Although previous opinion [17] has not regarded partial molecular attachment of extended chains, i.e. interfacial condition, as noticeably affecting their transport or the growth rate, the small perturbation we now see does not necessarily conflict with that broader view but, in any event, intimates that the processes whereby molecules attach to crystal interfaces are more subtle than is commonly assumed.

There is also increased support for the role of ciliation in spherulitic growth, which was the primary reason for undertaking this investigation. We have established previously in $C_{294}$ [14,15] and other *n*-alkanes [20] that when once-folded crystallization changes to extended-chain growth, there is a striking concomitant change in textural organization. The microstructure in the former is akin to that in polymers with spherulites constructed on a dominant/subsidiary scheme while the latter has extensive stacks of parallel lamellae and no spherulites, at least in the region of the changeover. Such stacks are omnipresent, as in, e.g. Fig. 2a, for extended-chain growth at low supercoolings, but one

Table 3
Key data for $C_{264}$ (this paraffin was melted at 134°C)

| Crystallization temperature (°C) | Growth rate (μm/s) | Crystallization time | Object diameter (μm) | Melting peak (°C) | Form |
|---|---|---|---|---|---|
| Quenched | | | 20–30 | 131.3 | once–fold. |
| 123 | 0.27 ± 0.01 | 2–3 min | 40–50 | 131.3 | mixed. |
| 124 | 0.29 ± 0.01 | 4–5 min | 50–60 | 131.5 | ext. |
| 125 | 0.30 ± 0.01 | 6–8 min | 70–90 | 131.9 | ext. |
| 126 | 0.25 ± 0.01 | 8–10 min | 100–130 | 131.9 | ext. |
| 127 | 0.14 ± 0.01 | 10–20 min | 140–160 | 131.8 | ext. |
| 128 | 0.056 ± 0.002 | 50–70 min | 400–600 | 131.1 | ext. |

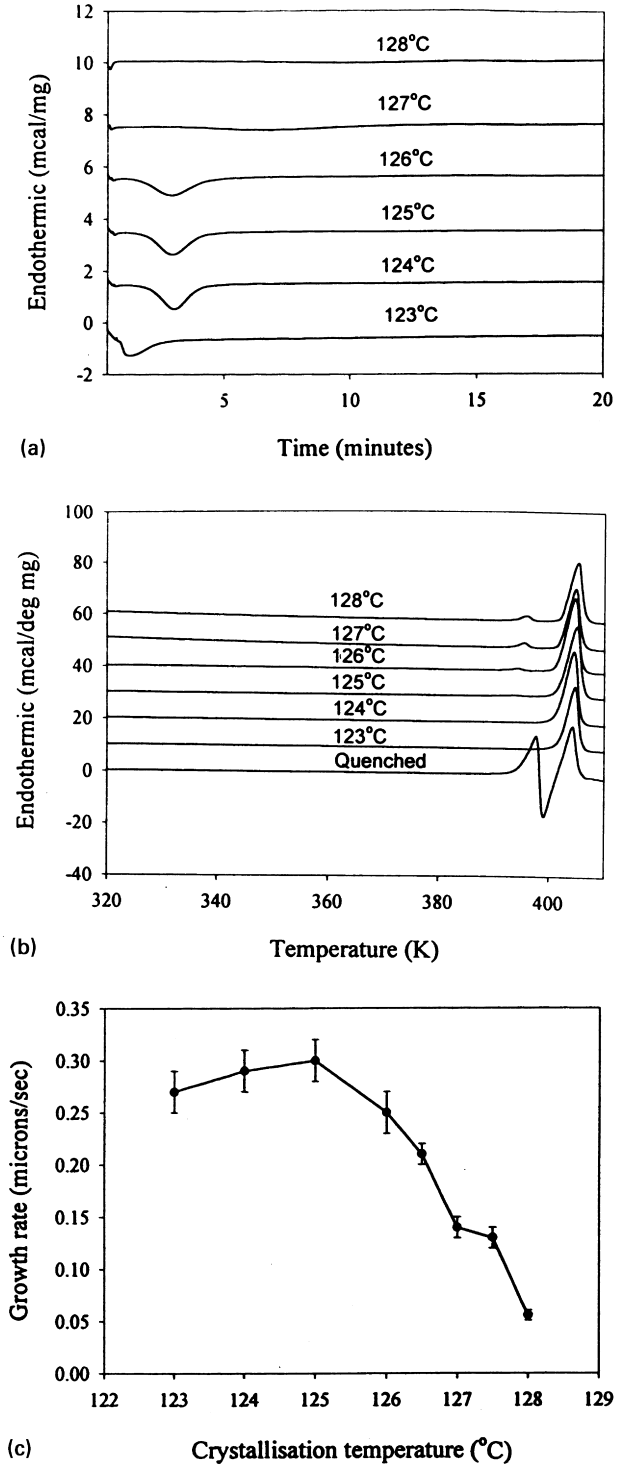


Fig. 7. Crystallization behaviour of $C_{246}$: (a) crystallization exotherms; (b) melting endotherms; and (c) growth rate plotted as a function of crystallization temperature.

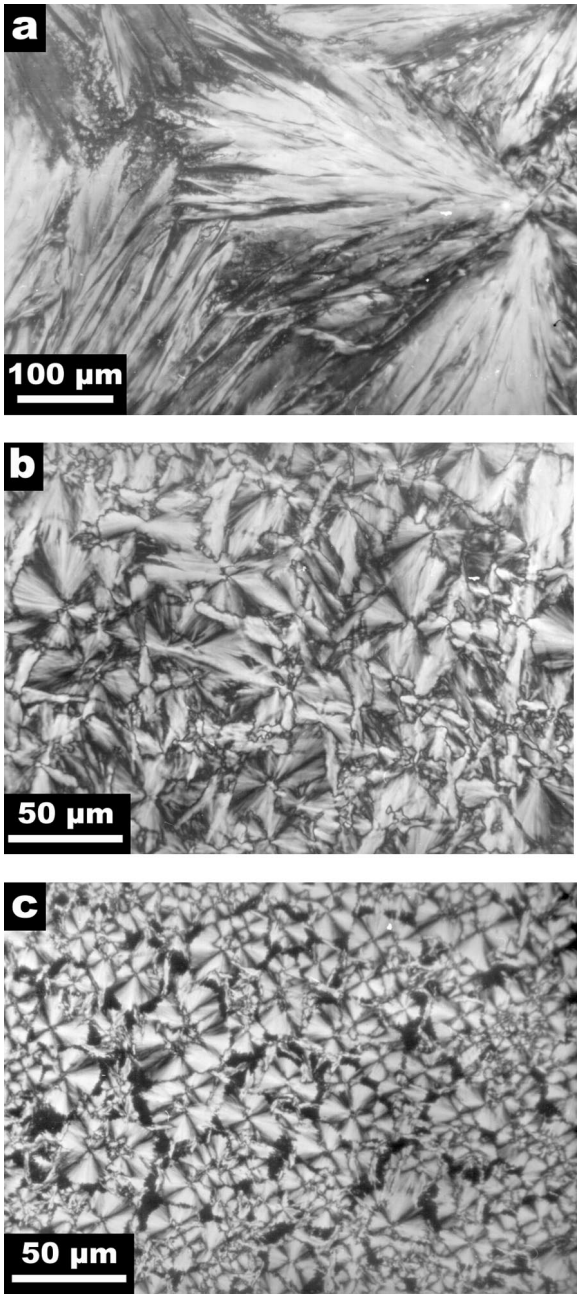


Fig. 8. Optical micrographs of $C_{246}$: (a) parallel groups of lamellae after crystallizing at 128°C; (b) a more disordered texture after crystallizing at 124°C; and (c) spherulitic texture produced after quenching.

needs to account for the introduction of branching and quasi-spherulitic textures at lower temperatures.

At this point one needs to point out that familiar existing terminology is unable to cater for the variations of 'spherulitic' textures shown in Figs. 2, 5 and 8. One moves from single lamellar textures through objects in which growth has nucleated centrally (with multiple orientations, then developed outwards but lacking the branching to fill space) eventually to finer textures when branching is both present and more copious. At the optical level, the appearance between crossed polars of the intermediate objects changes with the angle of rotation as more or less extensive regions extinguish as a whole, i.e. radii are no longer equivalent as in a classic spherulite. This is because of the presence of the parallel lamellar stacks associated with dominant lamellae, which are such a feature of extended-chain growth. Only

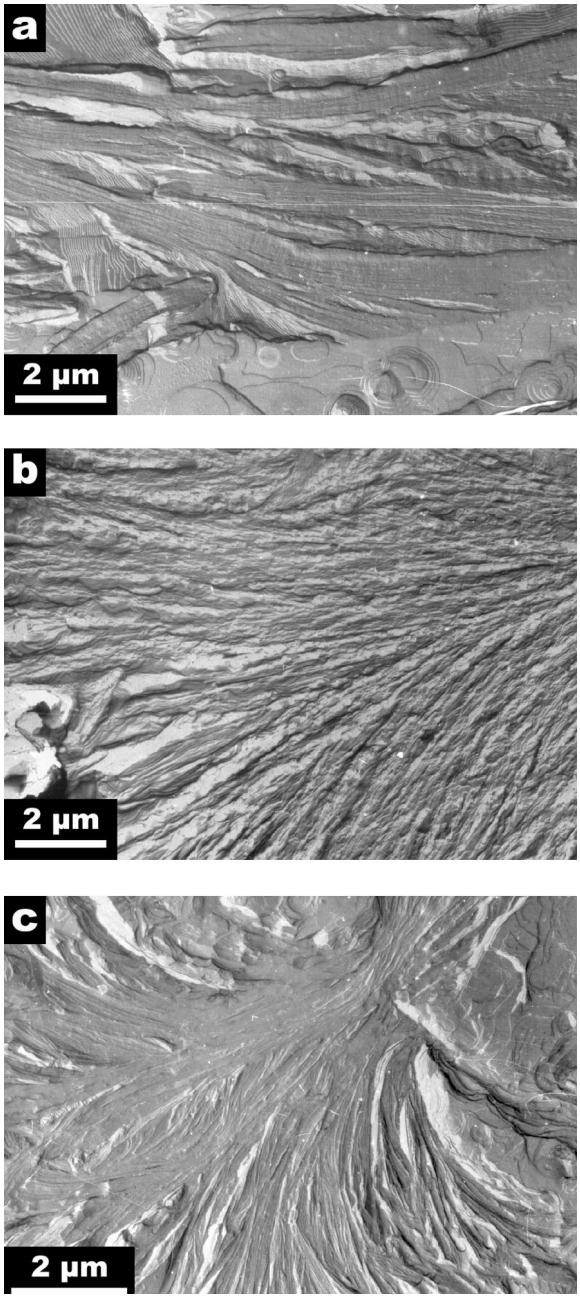


Fig. 9. TEM images of $C_{246}$: (a) morphology composed of parallel groups of crystals in a specimen crystallized at 119.2°C; (b) low angle divergent lamellar bundles produced by crystallizing at 123°C; and (c) example of spherulitic object produced by quenching.

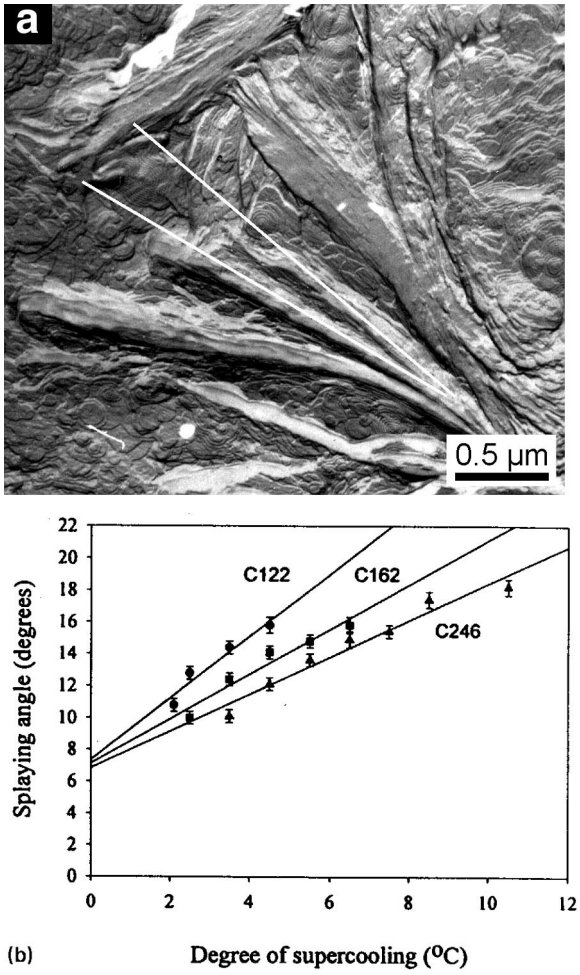


Fig. 10. (a) a magnified portion of Fig. 3c showing how angles of splay are measured; (b) lamellar divergence angle plotted as a function of supercooling for all three paraffins, with 'best fit' regression lines and standard deviations indicated on each data point.

when dominants branch more frequently does the optical appearance approach that of the typical spherulites found for chain-folded *n*-alkanes and polyethylene.

The cause of the branching observed for extended-chain lamellae at higher supercoolings, $\Delta T$, has been suggested to be transient ciliation due to the partial attachment. Because the size of the secondary nucleus varies as $1/\Delta T$, the potential cilium length, i.e. the excess of the molecular length, $L$, over that of the secondary nucleus will be approximately [16]

$$L(1 - \Delta T_0/\Delta T)$$

where $\Delta T_0$ is the minimum supercooling for finite growth rate. Fig. 10b shows that angles of splay (measured as in Fig. 10a, with error bars the width of 1 standard deviation) have the form of this relationship. It is easy to see that: (a) splaying angle scales linearly with supercooling in each case: and (b) the corresponding angle for the given supercooling become smaller for longer paraffins, as would be expected for the different lamellar thickness. While much more needs to be known before definitive answers can be put forward, this sort of behaviour supports the idea of 'transient ciliation' being responsible for lamellar divergence in extended-chain paraffins.

It is not a major objection to the role of ciliation that there are circumstances in which inorganic materials may form spherulites; these are, in general, both complex and poorly documented. Those of ice grown from aqueous glycerine solution [22] also have a morphology of diverging units

that has been proposed to be a response to short-range pressure, in this case from osmosis [23]. Spherulitic growth of apparently simpler inorganic systems but in complex circumstances, poses no inherent contradiction to the concept that the characteristic spherulitic growth of polymers is a consequence of ciliation, i.e. their molecular length.

## 5. Conclusions

There are four principal conclusions of this work:

1. The rate of extended-chain crystallization of *n*-alkanes increases linearly with supercooling in accordance with Hoffman's theory [17].
2. There is a local dip in the kinetics at the onset of lamellar branching.
3. In all the three paraffins, similar morphologies were observed at the same supercooling and the same progressive changes of texture with crystallization temperature. This is, with increasing supercooling, from a morphology composed essentially of individual lamellae arranged in parallel stacks and radiating from common nuclei through coarse, somewhat branched microstructures whose parallel stacks diverge, to finer, more-branched pseudo-spherulitic textures. Quenched, once-folded, $C_{246}$ shows a random spherulitic texture with a dominant/subsidiary microstructure as for polymeric systems.
4. Splaying angles increase with supercooling for all the three *n*-alkanes studied but are less, for the same supercooling, for the longer homologues with thicker lamellae, as would be expected of transient ciliation due to the excess of molecular length over that of the secondary nucleus, thereby reinforcing previous evidence showing the responsibility of ciliation for spherulitic development.

## Acknowledgements

This research was funded by EPSRC under whose auspices the *n*-alkanes were synthesized and supplied by Dr G.M. Brooke and colleagues of the University of Durham.

## References

[1] Keller A. Makromol Chem 1959;34:1–28.
[2] Bassett DC, Keller A. Proceedings of the European Regional Conference on Electron Microscopy. Delft, vol. 1, 1960. p. 284–8.
[3] Keller A. Philos Mag 1960;6:329–43.
[4] Bassett DC, Keller A. Philos Mag 1960;6:435–58.
[5] Paynter OI, Simmonds DJ, Whiting MC. J Chem Soc, Chem Commun 1982:1165–6.
[6] Bidd I, Holdup DW, Whiting MC. J Chem Soc, Perkin Trans 1987;1:2455–63.
[7] Bassett DC. CRC Crit Rev Solid State Mater Sci 1984;12:97–163.
[8] Bassett DC, Olley RH. Polymer 1984;25:935–43.
[9] Bassett DC, Vaughan AS. Polymer 1985;26:717–25.
[10] Patel D, Bassett DC. Proc R Soc London A 1994;445:577–95.
[11] Bassett DC, Olley RH, al Raheil IAM. Polymer 1988;29:1539–43.
[12] Ungar G, Stejny J, Keller A, Bidd I, Whiting MC. Science 1985;229:386–9.
[13] Sutton SJ, Vaughan AS, Bassett DC. Polymer 1996;37:5735–8.
[14] Bassett DC, Olley RH, Sutton SJ, Vaughan AS. Macromolecules 1996;29:1852–3.
[15] Bassett DC, Olley RH, Sutton SJ, Vaughan AS. Polymer 1996;37:4993–7.
[16] Teckoe J, Bassett DC. Polymer 2000;41:1953–7.
[17] Hoffman JD. Macromolecules 1985;18:772–86.
[18] Broadhurst MG. J Res Natl Bur Stand, USA 1962;66A:241–9.
[19] Hoffman JD. Polymer 1991;32:2828–41.
[20] White HM, Bassett DC. Unpublished work.
[21] Ungar G, Keller A. Polymer 1987;28:1899–907.
[22] Luyet BJ. Proc R Soc London B 1957;147:434–51.
[23] Geering GT. PhD thesis, Stanford, 1968, cited in Tiller WA. The science of crystallization: macroscopic phenomena and defect generation. Cambridge: Cambridge University Press, 1991. p. 345.